Kinetics and Mechanism of the Reaction of the Hydroxyl Radical with h_8-Isoprene and d_8-Isoprene: Isoprene Absorption Cross Sections, Rate Coefficients, and the Mechanism of Hydroperoxyl Radical Production

P. Campuzano-Jost, M. B. Williams, L. D'Ottone, and A. J. Hynes*

Division of Marine and Atmospheric Chemistry, Rosenstiel School of Marine and Atmospheric Science, 4600 Rickenbacker Causeway, Miami, Florida 33149-1098

Received: August 8, 2003; In Final Form: November 17, 2003

We have employed a pulsed laser photolysis−pulsed laser induced fluorescence technique to study the kinetics and mechanism of the reaction of OH with isoprene. Three isotopomeric variants of the reaction have been studied. A rate coefficient of $(8.47 \pm 0.59) \times 10^{-11}$ cm^3 molecule^{-1} s^{-1} ($\pm 2\sigma$) was obtained at room temperature and showed no kinetic isotope effect within the precision of the measurements. The rate coefficient was independent of pressure over the range of 60−600 Torr and showed no dependence on the nature of the buffer gas in nitrogen, air, and helium. A limited study of the temperature dependence indicated that the reaction displays a slight negative activation energy ($E_a = -690$ J/mol). The gas-phase ultraviolet absorption spectrum of both regular and deuterated isoprene was obtained at room temperature and showed a strong absorption feature in the far ultraviolet. The absolute absorption cross section at ∼215 nm, the absorption peak, is $\sim 7 \times 10^{-17}$ cm^2. The detailed oxidation mechanism was examined by experiments in which NO was added to the gas mixture in order to recycle product HO_2 to OH. At least 20 OH temporal profiles were obtained for each of the 3 isotopomeric variants. The profiles were modeled using the current isoprene module of the master chemical mechanism (MCM) that has been developed at Leeds University. The MCM mechanism gave good fits to the experimental profiles for all three reactions. A sensitivity analysis was developed to examine the extent to which recycling experiments can constrain individual rate coefficients in the MCM reaction mechanism. We obtain a lower limit of 4×10^{-12} cm^3 molecule^{-1} s^{-1} for the rate coefficient for the addition of O_2 to the hydroxyalkyl radical formed by OH addition to isoprene. Our results suggest that uncertainties in the database on NO radical termination steps are a major limitation in the ability of recycling experiments to constrain the MCM mechanism.

Introduction

Isoprene is the primary component of the atmospheric burden of nonmethane hydrocarbons. On the basis of current emission estimates, isoprene constitutes approximately 44% of the total NMHC emissions inventory.[1] The primary production sources of isoprene are natural, with deciduous trees being large emitters.[2] However, the discovery that phytoplankton produce isoprene suggests that isoprene may be a ubiquitous feature of atmospheric chemistry in the tropospheric boundary layer.[3−5] Interest in the atmospheric chemistry of isoprene is related to its importance in the background chemistry of the unpolluted atmosphere[6,7] and also to the significant role that natural isoprene emissions can play in urban pollution episodes that lead to ozone formation.[8−10] The initial step in the atmospheric degradation may involve reaction with OH, O_3, or NO_3; however, reaction with OH, reaction R1, is the primary channel under most circumstances:[1,11]

$$OH + C_5H_8 \rightarrow OHC_5H_8 \quad (1)$$

As a result of this, a large number of chamber investigations have focused on the chemistry of the OH-initiated degradation of isoprene, inferring the mechanism from product studies.[12−17] A number of oxidation mechanisms have appeared that contain the detailed oxidation steps together with appropriate rate coefficients, most of which are inferred from structural additivity relationships or ab initio calculations.[11,18−20] There are few measurements of any of the intermediate oxidation steps.

Although there have been several relative rate studies of the rate coefficient for R1, until recently direct studies were limited. In this work, our goal was to measure the rate coefficient directly under a variety of conditions, including those typical of the troposphere. We reported a preliminary account of a direct determination of the rate coefficients for R1 and its isotopic variants, reactions R2 and R3, together with studies of the recycling of product HO_2/DO_2 in the presence of NO.[21]

$$OD + C_5H_8 \rightarrow ODC_5H_8 \quad (2)$$

$$OH + C_5D_8 \rightarrow OHC_5H_8 \quad (3)$$

Since that publication, several experimental and theoretical studies focusing on both the absolute rate of the reaction and the detailed mechanism of the degradation process have appeared.[15,22−35] We have revisited the absorption cross sections of h_8-isoprene and d_8-isoprene at high spectral resolution between 205 and 230 nm, constraining the largest uncertainty in our kinetic measurements, and present them here together with the full details of our kinetics studies, including a comparison with recently reported studies.

* Corresponding author. E-mail: ahynes@rsmas.miami.edu.

10.1021/jp0363601 CCC: $27.50
Published on Web 02/10/2004

In addition, we detail the experiments and model employed to monitor the subsequent progress of isoprene degradation, allowing us to constrain proposed reaction mechanisms and determine rate coefficients for some intermediate steps. We do this by monitoring the recycling of product HO_2 back to reactant OH in the presence of NO:

$$HO_2 + NO \rightarrow OH + NO_2 \qquad (4)$$

Although our ability to constrain the rate coefficients of individual mechanistic steps is limited, we find that our observations agree well with the predictions of the isoprene module of the master chemical mechanism developed at the University of Leeds.[14,18,36]

Experimental Section

Absorption Cross Sections. In experiments reported previously, the absorption cross sections at 228.9 nm were measured in a series of experiments in which a known pressure of h_8-isoprene or d_8-isoprene was introduced into an absorption cell and the attenuation of the 228.9-nm line from a Cd discharge lamp was monitored using a photomultiplier/band-pass filter combination.[21] To confirm these experimental results, we measured absorption cross sections between 205 and 230 nm at higher spectral resolution. h_8-Isoprene or d_8-isoprene mixtures, typically 1% in 1000 Torr total pressure, were made up manometrically in large Pyrex storage bulbs using a different set of capacitance manometers from those used in the prior experiments. A deuterium lamp (Hamamatsu L979-01) served as the light source. The light passed through a 100-cm absorption cell, was dispersed by a 0.5-m spectrograph (Jobin-Ivon HR640), was detected by a 1024-element photodiode array (EG&G M1421), and was processed by an optical multichannel analyzer (OMA, EG&G M1463). The wavelength scale was calibrated using the atomic lines from Zn and Cd lamps (BHK Inc). With a 3000 lines/mm spectrometer grating, we obtained a resolution of ~0.05 nm, taken from the fwhm of isolated atomic lines.

Kinetics. Our use of the PLP-PLIF technique for the study of hydroxyl radical kinetics has been described previously,[37] and a brief review of the experimental configuration in this work is given below. Experiments were performed in a Pyrex cell. The central 25-cm-long section of the cell was jacketed to permit the flow of heating or cooling fluid from a thermostated bath. A copper−constantan thermocouple with a stainless steel jacket was inserted into the reaction zone through a vacuum seal, allowing the measurement of the gas temperature under the precise pressure and flow conditions of the experiment. The photolysis and probe lasers counterpropagated through side windows across the direction of gas flow. Fluorescence was detected through a third sidearm, perpendicular to the photolysis and probe beams. OH was produced by the pulsed laser photolysis of H_2O_2 or HNO_3 using the 266-nm fourth harmonic of a Nd:YAG laser (Quanta Ray GCR-4). OD was produced by the photolysis of DNO_3. Pulsed laser induced fluorescence using a Nd:YAG-pumped, frequency-doubled dye laser (Quanta Ray DCR-3/PDL-3) was used for OH and OD detection. Excitation was via the Q_11 line of the A−X (1−0) transition at 282 nm for OH and 287 nm for OD. Fluorescence in the 0−0 and 1−1 bands was detected by a photomultiplier after passing through collection optics and filters to discriminate against Rayleigh scattering and Raman scattering from N_2 and/or O_2. The photomultiplier output was appropriately terminated and fed to a 500-MHz digital oscilloscope to obtain integrated voltage averaged for (typically) 100 laser shots. Kinetic information was obtained by varying the delay between the photolysis and probe lasers using a digital delay generator. The signal was collected for an appropriate number of delay times in order to map out a complete OH temporal profile. All experiments were carried out under slow flow conditions to avoid the buildup of reaction products. All flows were monitored using calibrated mass flowmeters. Partial pressures of O_2 and NO were calculated from flows. Dilute mixtures of C_5H_8 and C_5D_8 were made up manometrically in large glass storage bulbs. Concentrations of C_5H_8 and C_5D_8 were calculated from flows and measured in situ by photometry using the 228.9-nm line of a Cd lamp.[61] The attenuation of the 228.9-nm line was monitored both before and after the absorption cells using a photomultiplier and a narrow band-pass dichroic filter. Concentrations calculated using both approaches were in good agreement. Concentrations obtained from photometry were used in all calculations because we believe that they improve both the accuracy and precision of the rate coefficients obtained.

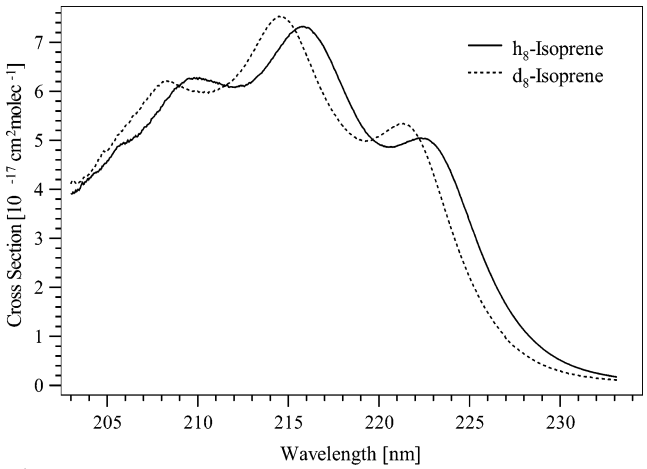

Figure 1. UV spectra of h_8- and d_8-isoprene.

The pure gases and chemicals used in this study had the following stated minimum purities: N_2 (99.999%), He (99.996%), O_2 (99.99%), and synthetic air (99.99%) were obtained from Praxair. H_2O_2 (70%) was obtained from FMC corporation; it was further concentrated and purified by bubbling buffer gas through the sample for several days before use in experiments. h_8-Isoprene (>99%) and nitric acid (70% azeotrope in water) were obtained from Aldrich Chemicals, d_8-isoprene (>98%), from Cambridge Isotope Labs, and *d*-nitric acid (99% D), from Aldrich Chemicals.

Results and Discussion

Absorption Spectrum and Absolute Absorption Cross Sections. Figure 1 shows the absorption spectra of C_5H_8 and C_5D_8. Table S1, listing the absorption cross sections as a function of wavelength, is included in the Supporting Information. Our high-resolution data show that the spectrum of deuterated isoprene is blue-shifted by approximately 1.25 nm. For C_5H_8, the absolute value of the absorption cross section at 228.1 nm is 8.29×10^{-18} cm^2, within 1% of our previously reported value. For C_5D_8, we obtain 4.65×10^{-18} cm^2, approximately 4% lower than our previous value. It is worth noting that no buildup of a polymerization product was observed for the diluted samples, in sharp contrast with the measurements with pure isoprene reported before. This might be due to the lower partial isoprene pressures used or to the suppression of wall reactions at the higher total pressures used in the diluted experiments. That both determinations yield almost identical

TABLE 1: Determinations of k_1, k_2, and k_3

p [Torr]	bath gas	T [K]	k [10^{-11} cm^3 molecule^{-1} s^{-1}]	dk [10^{-11} cm^3 molecule^{-1} s^{-1}]	$k(T)$ [10^{-11} cm^3 molecule^{-1} s^{-1}]	d$k(T)$ [10^{-11} cm^3 molecule^{-1} s^{-1}]
			OH + h_8-Isoprene			
200			8.27	0.161		
615	He		8.55	0.144		
72			8.68	0.189		
200			8.58	0.171		
60	air		7.76	0.154		
600			8.37	0.206		
200		297	8.78	0.178	8.47	0.64
50			8.24	0.204		
600			8.94	0.133		
600			8.76	0.130		
			8.17	0.165		
	N_2		8.35	0.165		
			8.71	0.141		
200		276	9.13	0.180	9.13	0.180
		262	9.15	0.181	9.15	0.181
		251	9.87	0.254	9.87	0.254
		320	7.39	0.140	7.39	0.140
		342	6.73	0.139	6.73	0.139
			OD + h_8-Isoprene			
200	N_2	297	8.45	0.177	8.43	0.18
			8.42	0.163		
			OH + d_8-Isoprene			
200	N_2	297	8.27	0.166	8.27	0.17

results suggests that the error associated with polymerization is negligible. Therefore, we think that the total error for the UV cross section, and hence for the isoprene concentration determination in the kinetic experiments, amounts mainly to the precision of the manometric determination of the isoprene concentration, which is around 5%.

The only previous literature data is a slightly lower resolution spectrum of C_5H_8 reported by Jones and Taylor almost 50 years ago.[38] The Jones and Taylor spectrum is plotted on a logarithmic absorptivity scale with four other dienes, and although it is similar to ours, accurate values are difficult to interpolate. One absorbance value in our range of interest, however, is shown in a table with literature comparisons. They measured a molar absorptivity of 19 800 L mol^{-1} cm^{-1}, corresponding to a cross section of 7.6×10^{-17} cm^2, at 215.5 nm. At this wavelength, we obtain a value of 7.3×10^{-17} cm^2, a difference of merely 4%. This is well within the experimental uncertainty of our measurements and gives us further confidence in the accuracy of our isoprene concentration measurements during the kinetic experiments.

Kinetic Studies. All standard kinetic experiments were performed under pseudo-first-order conditions. The concentration of isoprene was varied between 1×10^{14} and 2×10^{15} cm^{-3} and was in large excess over that of OH, which was typically around 1×10^{12} cm^{-3}. Under these conditions, the observed OH decays should follow simple first-order kinetics:

$$\ln\left(\frac{[\mathrm{OH}]}{[\mathrm{OH}]_0}\right) = (k_1[\text{isoprene}] + k_\mathrm{D})t = k't$$

where k_1 is the bimolecular rate coefficient for R1 and k_D is the first-order rate coefficient for the loss of OH by diffusion from the detector field of view and background reaction. Examples of temporal profiles of OH for R1 have been shown previously. All data for both OH and OD was of high quality with the pseudo-first-order decay rates, determined over at least 3 and typically 4 to 5 $^1/_e$ times, showing 2σ uncertainties of 2%. No deviation from pseudo-first-order behavior was observed, indicating the absence of complications from secondary chemistry. This implies that the lifetime of the OH−isoprene adduct is much longer than the time scale of our experiments and that the adduct does not react with O_2 to produce OH as a reaction product. In all, 17 determinations of rate coefficients for R1 were performed over the pressure range of 60−600 Torr at 6 temperatures between 251 and 242 K. In addition, three determinations of the rate coefficients for R2 and R3 were performed at 298 K. The kinetic data set is summarized in Table 1.

The rate coefficients listed in Table 1 are clearly consistent with the conventional view of the OH-initiated oxidation mechanism as proceeding via the addition of OH to one of the double bonds to form a stable adduct. The rate coefficients for R1, R2, and R3 are equal within the precision of our measurements, and this, together with the mechanistic studies detailed below, suggests that the reaction proceeds exclusively by addition with no significant abstraction component. The rate coefficients are independent of both pressure and the nature of the buffer gas, indicating that the addition reaction has reached its high-pressure limit at 60 Torr over the range of temperatures used in this work. Because the measured rate coefficients are independent of both pressure and buffer gas, the measurements at each temperature have been averaged, and these averaged values are also reported in Table 1.

Recent experiments in our laboratory have shown that instabilities in the absorption measurements are the main source of the statistical error of the rate coefficients. A weighted fit to the data using only the precision error of the LIF decays not only underestimates the total error but also can bias the result of the fit. Therefore, we have undertaken a reanalysis of all of our kinetic data, including conservative estimates for the precision error of the concentration, derived from current measurements on the same apparatus. We have also checked for consistency between weighted and unweighted fitting procedures, discarding data where the difference was greater than 5% as a result of significant variation in lamp intensity during the course of an experiment. This gives a new average of the measurements for the rate coefficient at 297 K of 8.47×10^{-11} cm^3 molecule^{-1} s^{-1} with a 2σ regression error of $0.59 \times$

TABLE 2: Summary of Published Kinetic Studies on the OH + Isoprene Reaction

author	k [10^{-11} cm^3 molecule^{-1} s^{-1}]	Dk [10^{-11} cm^3 molecule^{-1} s^{-1}]	pressure/gas	[isoprene] [10^{11} molecule cm^3]	[OH]/ [isoprene]	detection method
Atkinson et al.[12]	9.98	0.45	760 Torr air			relative rate GC propene
Atkinson and Aschmann[57]	10.2	0.4	760 Torr air			relative rate GC propene
Ohta[58]	9.9	0.27	760 Torr air			relative rate GC 1,3-butadiene
Edney et al.[59]	10.1	0.2	760 Torr air			relative rate GC propene
Gill and Hites[24]	10.1	1.9	760 Torr He			relative rate MS 2-methyl-propene
Cox et al.[60]	7.8	~0.8	760 Torr air			relative rate GC ethene
Kleindienst et al.[40]	9.26	1.5	50−200 Torr Ar	10−60	unknown	FP-RF
Siese et al.[52]	9.7		unknown	unknown	unknown	FP-RF
Donahue et al. (private commun.)	8.13	0.1	unknown	unknown	unknown	TFT/LIF (^{18}OH)
Choung and Stevens[35]	11.0	0.5	2−6 Torr He	4−16	3−15	DF/LIF
Choung and Stevens[26]	10.8	0.5	100−150 Torr Ar	2−20	3−15	TFT/LIF
McGivern et al.[32]	9.9	0.5	20 Torr Ar	1000−10 000	5000−50 000	PLP/LIF
Zhang et al.[29]	10.1	0.8	70−120 Torr N_2	3−50	40−100	TFT/CIMS
this work	8.47	0.64	60−600 Torr	10 000−15 000	100−1500	PLP/LIF

10^{-11}. As a testimony to the robustness of the data set, the new value is within 1% of the one reported before. The new statistical error is about 5 times the one calculated from LIF precision alone and should be regarded as a fairly conservative estimate.

This value for the rate coefficient is 15% below the rate coefficient of 1×10^{-10} cm^3 molecule^{-1} s^{-1} currently recommended by the IUPAC panel[39] and lies at the low end of reported rate coefficients that lie between 7.7×10^{-11} and 11.1×10^{-11} cm^3 molecule^{-1} s^{-1} and are summarized in Table 2. The two sources of potential systematic error in this type of study occur in the determination of the pseudo-first-order rate of OH and the determination of the concentration of the excess reactant, isoprene. The ratio [isoprene]/[OH] used in this work is significantly larger than in any other direct study. This, together with the low initial concentrations of OH used, should minimize the possibility of secondary chemistry contributing to the observed OH decay rate. As we note above, we believe that in situ monitoring of reactant concentrations by photometry both increases precision and minimizes the possibility of systematic error resulting from incorrect concentration measurement. In this work, we measured concentrations before and after the reaction cell and obtained the same value, indicating that there was no loss of isoprene to the reactor walls. In some cases, a multichannel analyzer was used to obtain the spectrum of the reactant mixture, and there was no suggestion of any "dark" chemistry. This suggests that problems related to the polymerization of isoprene in the flowing gas mixture are negligible. We believe that the agreement we obtain for the rates of R1 and R2 implies that our estimate of our overall accuracy (an uncertainty of less than 10%) is realistic.

An accurate and precise value of the rate coefficient for R1 is particularly important because in certain circumstances isoprene can act as a significant sink for OH. Hence, uncertainties in this rate coefficient will impact not only isoprene chemistry but also the partitioning between major OH sinks.

Compared to the other direct determinations in the literature, only Kleindienst et al.'s 1983 data falls within our estimated error limits.[40] The unpublished data of Donahue et al., reported in our last paper, is in excellent agreement, although these results are from a limited number of experiments. The measurements from Choung and Stevens and the Texas A&M groups of North and Zhang reported in the last 3 years all lie 15−25% higher than the measurements reported in this work.[23,26,27,29,31,32,35,41] The reasons for this discrepancy are unclear. Chuong and Stevens studied R1 at low pressure in He and report a rate coefficient of 11.0×10^{-11} cm^3 molecule^{-1} s^{-1} at 2, 4, and 6 Torr, although the addition of O_2 was required to suppress heterogeneous chemistry. In a subsequent study in argon in a turbulent-flow reactor, they obtained essentially the same result. Zhang, North, and co-workers studied R1 using both turbulent-flow reactor and laser photolysis/LIF techniques. They obtained a value of 10.1×10^{-11} cm^3 molecule^{-1} s^{-1} at six pressures between 70 and 120 Torr in a N_2 buffer using the turbulent-flow reactor. They reported laser photolysis/LIF experiments over the range of 0.5−20 Torr in Ar that gave a high-pressure limit of $9.9 \times 1\ 0^{-11}$ cm^3 molecule^{-1} s^{-1}. Their low-pressure studies disagree with the low-pressure study of Chuong and Stevens in that they found a pressure dependence below 10 Torr. The limited range of pseudo-first-order rates measurable in flow tubes resulted in the use of relatively low isoprene/OH ratios in those studies. The laser photolysis/LIF studied used higher ratios similar to those used in this work. In contrast to our work, McGivern et al. used the 193-nm photolysis of HNO_3 as the OH precursor. As they note, isoprene absorbs at this wavelength, and the photolysis of HNO_3 produces both OH and O^1D. They inferred isoprene concentrations by passing Ar over isoprene liquid, assumed saturation, and calculated concentrations from the isoprene vapor pressure.

As shown in Table 2, there have been several measurements of k_1 at atmospheric pressure in air using relative rate approaches, mostly relative to the reaction of OH with propene. These results are in good agreement with the higher value of 1×10^{-10} cm^3 molecule^{-1} s^{-1} for k_1.[42] Our lower value for k_1 also implies that either the currently recommended value for OH + propene is 15% too high or some unidentified secondary chemistry is affecting the isoprene studies.

Figure 2 shows an Arrhenius plot of our data together with all other direct studies and temperature-dependent measurements that have been reported in the literature to date. As can be seen, the slopes of the temperature dependencies determined by Kleindienst et al., Gill and Hites, and us are all very similar, perhaps an indication that systematic errors in concentration measurements and not kinetic detection artifacts are responsible for the discrepancy in the absolute values for the rate coefficient of R1. The slope of the Arrhenius plot reported here is slightly smaller than the values from Kleindienst et al. and Gill and Hites and is mainly due to the measurements in the range below 298 K not covered by the other two groups; however, all three values agree well within our conservative error estimates:

$$k_1(250-340\ \mathrm{K}) = (8.63 \pm 0.42) \times 10^{-11} \cdot \exp\left((348 \pm 136) \cdot \left(\frac{1}{T} - \frac{1}{298\ \mathrm{K}}\right)\right) \mathrm{cm}^3\ \mathrm{s}^{-1}$$

OH Regeneration Experiments. *General Approach.* The OH cycling experiments were performed at a total pressure of 200

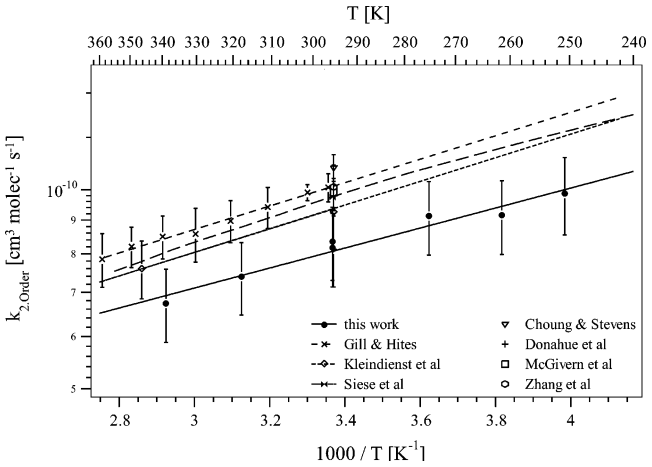

Figure 2. Arrhenius-style plot of the temperature dependency of k_1 found in this work and in the literature.

Torr in N_2 buffer gas at room temperature. Relatively high isoprene and NO concentrations were used, compared with those typically seen in chamber experiments. Two main considerations led to the choice of these experimental conditions. It was necessary to operate in a configuration that allowed a sufficiently high signal-to-noise ratio to produce well-defined kinetic decays when the OH concentration had dropped to between 10 and 1% of its initial value but at pressure high enough to ensure that most pressure-dependent reaction rates were close to their values under atmospheric conditions. It was also desirable to make the main oxidation pathway sufficiently rapid that cross reactions and slow rearrangements of the intermediates did not need to be factored into the chemical modeling. In addition to this, higher concentrations resulted in smaller errors in the determination of isoprene and NO mixing ratios, greatly reducing uncertainties in the highly nonlinear simulation runs.

Identical experiments were performed for R1−R3. Four different isoprene/NO ratios were used, and oxygen concentrations were varied over an order of magnitude in order to obtain a series of nonexponential decays for each reaction. OH concentrations reached equilibrium at levels of 1−10% of the initial concentration on time scales between 60 and 300 μs. Twenty reactions profiles were obtained for R1, and twenty-four profiles were obtained for R2 and R3. Table 3 sums up the experimental conditions for all of the OH cycling experiments. For NO, the agreement between the concentrations calculated from the kinetics in the absence of isoprene and the ones calculated from flows was excellent. Isoprene concentrations calculated from optical absorption in the absence of NO were consistent with the kinetic rates observed using the rate coefficient determined in this work. Concentrations varied by less than 5% over the course of an experiment. For each set of fixed NO/isoprene concentrations, all LIF profiles were first normalized in order to account both for probe power fluctuations and OH quenching at higher O_2 mixing ratios; corrections were typically less than 15%. The photolysis laser power was stable to within 5%. The LIF signal profiles were then converted to OH concentrations based on the average photolysis laser power and HNO_3 concentration. For each reaction, a single chemical mechanism was then used to reproduce the data for all four experimental sets of conditions. No least-squares fitting was performed; rate coefficients were varied until the best visual overlap between simulation and data was achieved.

Methane Experiments. To test the ability of our system to monitor realistic OH regeneration rates at the chosen conditions, a set of experiments were performed substituting methane for isoprene. The oxidation of methane, although still not completely understood, relies on a much larger body of kinetic evidence, so it seemed feasible to model such curves within the constrains of the IUPAC recommendation.

Because both the initial step, OH + methane, and the formation of methylperoxy are very slow, high concentrations of methane and oxygen had to be used to achieve a significant HO_2 buildup on similar time scales to those observed in the isoprene experiments, although regeneration was still 2−5 times slower than for isoprene. Despite the fact that the initial step is an abstraction, not an addition, the mechanism for OH regeneration is similar to the one already described for isoprene and is summarized in Table S2. Using the recommended values, the simulated temporal profiles were slightly higher than those determined experimentally. By reducing the available methoxy concentration by 30%, either by decreasing the rate coefficient for methoxy formation, increasing the rate coefficient for NO depletion, or any combination of the two, a good match of the data could be achieved as shown in Figure S1. Depending on the combination of rates chosen, they fall within or just barely outside of the recommended confidence limits stated by the IUPAC recommendation.

TABLE 3: Experimental Conditions of the OH Regeneration Measurements

[NO] flow [10^{14} molecules cm^{-3}]	[NO] kin. [10^{14} molecules cm^{-3}]	[NO] used [10^{14} molecules cm^{-3}]	[isoprene] opt. [10^{14} molecules cm^{-3}]	[isoprene] kin. [10^{14} molecules cm^{-3}]	[isoprene] used [10^{14} molecules cm^{-3}]
		OH + h_8-Isoprene			
57	n.a.	57	9.4−10.0	10.0	9.8
11.5	n.a.	11.5	9.7−9.8	10.0	9.8
57	n.a.	57	2.65−2.82	3.0	2.8
11.5	n.a.	11.5	2.65−2.82	3.0	2.8
		OD + h_8-Isoprene			
47	46	47	8.8	8.6	8.8
7.7	7.8	7.7	8.8	8.6	8.8
47	46	47	2.4	2.6	2.4
7.0−7.7	n.a.	7.7	2.6	2.6	2.6
		OH + d_8-Isoprene			
43	46	43	9.4	9.5	9.4
7.2−8.0	10	7.6	9.4	9.5	9.4
43−47	45	43	2.5	2.7	2.5
7.2−8.0	n.a.	7.6	2.3	2.7	2.5
		OH + CH_4			
8.6−9.3	n.a.	8.8	15 000	10 800	12 000
3.8−4.2	3.9	4.0	7700	7900	7800

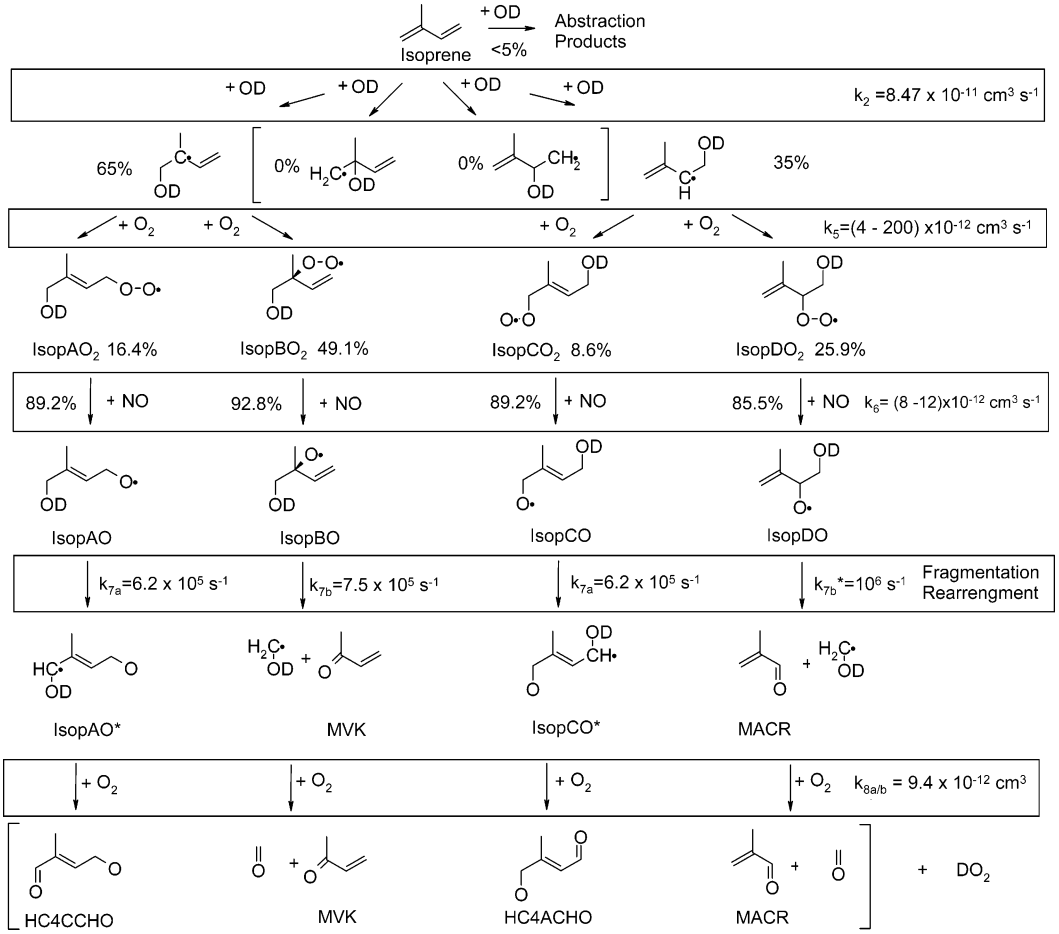

Figure 3. Schematic of the isoprene oxidation mechanism according to the MCM.[36]

Model Description: Isoprene Oxidation. The mechanism used is shown schematically in Figure 3 and is written for R2 explicitly tracking the initially added OD. It is based on the current isoprene module of the master chemical mechanism (MCM) that has been developed at Leeds University by Jenkin and co-workers.[14,18,36] This model assumes that the OH reaction proceeds exclusively via addition to the terminal carbons of the double bonds. Products of the addition to the secondary and tertiary carbons are disregarded to keep the overall number of isomers low. This is in line with most current estimates of the relative importance of these channels that are thought to account for less than 10% of the total reaction.[13,30,43,44] After the addition of O_2 to the terminal hydroxyalkene radicals, two β-hydroxyperoxy radicals ($IsopBO_2$, $IsopDO_2$ in Figure 1) are formed as the main products, along with two δ-hydroxyperoxy radicals ($IsopAO_2$, $IsopCO_2$) in smaller yields. This product distribution is predicted in principle by ab initio calculations,[30,31,43] but the actual yields for the β-hydroxyperoxydes in the Leeds model are based on the measured final ratios of the assumed products of the β-hydroxyperoxydes, methacrolein (MACR) and methylvinyl ketone (MVK).

Because the MCM model is designed to simulate atmospheric conditions and hence a partial pressure of oxygen of 150 Torr, the oxygen-dependent steps are implicit in the model. To be sensitive to these steps, much lower oxygen mixing ratios were used in this work. Oxygen-dependent separate steps R5, R8a, and R8b were included in the mechanism. To minimize the number of free parameters, the yields of the hydroxyperoxides from the MCM model were kept, and an isomer-independent oxygen addition step was added The rate coefficient k_5 was treated as a free parameter in our simulations. As a starting value, we used 8×10^{-12} cm^3 molecule^{-1} s^{-1}.

$$1,4\text{-}OHC_5H_8 + O_2 \rightarrow 0.75\beta\text{-}OHC_5H_8OO + 0.25\delta\text{-}OHC_5H_8OO \quad (5)$$

The four hydroperoxides can react with NO to form either β- and δ-hydroxyalkeneoxides, R6a, or hydroxynitrates, R6b:

$$\beta,\delta\text{-}OHC_5H_8OO + NO \rightarrow \beta,\delta\text{-}OHC_5H_8O + NO_2 \quad (6a)$$

$$OHC_5H_8OO + NO \rightarrow OHC_5H_8ONO_2 \quad (6b)$$

The nitrate formation is considered to be minor, with yields around 10% for all isomers, and amounts to a net loss process in our experiments. The main path, the formation of hydroxyalkeneoxides, is a fast process that has been studied several times in smog chambers; however, inferred rates are strongly dependent on assumptions made in the next step, fragmentation of the β-hydroxyalkeneoxides (IsopBO, IsopDO) or rearrangement of the δ-hydroxyalkeneoxides (IsopAO, IsopCO). Using the current MCM model,[36] current smog chamber data can be interpreted with a rate of formation of the hydroxy-alkeneoxide of 8×10^{-12} cm^3 molecule^{-1} s^{-1}. This value was used initially in the current model and then subjected to a sensitivity analysis.

In the MCM model, fragmentation of the β-hydroxyalkeneoxides (IsopBO, IsopDO) produces the main isoprene oxidation products, MACR and MVK, together with formaldehyde. In this work, the fragmentation step giving MACR, MVK, and methylenehydroxide (CH_2OH), R7a, and the reaction of CH_2-OH with oxygen to form formaldehyde and HO_2, R8a, are separate steps. The unimolecular rates for the fragmentation step

were made fast enough to ensure that they were not rate-determining under our conditions, which puts them in the range of 1×10^6 s^{-1}. This is in agreement with both the MCM values for typical atmospheric conditions and the structural additivity estimates from Atkinson[45] ($(1-16) \times 10^5$ s^{-1}) but higher than values obtained from other models.[23,26] Recent ab initio calculations, however, come up with very high values[28,43] (1×10^{12} and 1×10^8 s^{-1}). Given the size of the radicals involved, it is highly unlikely that these unimolecular rates at 760 Torr differ significantly from the 200 Torr rates appropriate here. R8a has been studied by Nesbitt et al. and Pagsberg et al.,[46-49] and on the basis of these studies, the IUPAC Panel has proposed a value of 9.6×10^{-12} cm^3 molecule^{-1} s^{-1} that was used here:[39]

$$\beta\text{-}OHC_5H_8O \rightarrow C_4H_6O + CH_2OH \quad (7a)$$

$$CH_2OH + O_2 \rightarrow HCHO + HO_2 \quad (8a)$$

By a 1,5-H-shift rearrangement, the δ-hydroxyalkeneoxides (IsopAO, IsopCO) form δ-di-hydroxyalkenes (IsopAO*, IsopCO*), followed by an H-abstraction step by oxygen that is again implicit in the MCM and produces γ-hydroxyalkenals. Again, two steps were included. As noted above, the rearrangement step was made fast enough to ensure that it was not rate-determining. We could not find any rate data for R8b, the abstraction/HO_2 formation step. It is unlikely that, given the current uncertainties in the simulation parameters, it would be possible to discern any isomeric effects, and as an initial estimate, the abstraction rate was set to be as fast as R8a:

$$\delta\text{-}OHC_5H_8O \rightarrow \alpha,\delta\text{-}(OH)_2C_5H_7 \quad (7b)$$

$$\alpha,\delta\text{-}(OH)_2C_5H_7 + O_2 \rightarrow \gamma\text{-}OHC_4H_6CHO + HO_2 \quad (8b)$$

The HO_2 (or DO_2 in the case of R2) formed in R8a and R8b can then be quickly converted under our experimental conditions back to OH (OD) via R4:

$$HO_2 + NO \rightarrow OH + NO_2 \quad (4)$$

The kinetics of R4 have been the subject of many studies and the rate coefficient is well characterized, so it was taken as a fixed parameter in our system.

It should be noted that the MCM also follows the further oxidation of MACR, MVK, and the δ-hydroxyalkenals. At the concentrations of isoprene used here, we assume that the oxidation of these products is negligible on the time scale of these experiments. In addition, the MCM includes cross reactions of the hydroalkeneperoxides, a full HO_x/NO_x module, and the reactions of OH with nitrates, peroxides, and oxides. All of these reactions were included in the current simulations; however, they are not needed to explain the experimental results.

Additional reactions of some intermediates with NO are required to explain the observed temporal profiles obtained at the highest NO concentrations used in this work. There is a single measurement of the rate coefficient for the reaction of CH_2OH with NO, obtained from a fit to a complex mechanism,[47,48]

$$CH_2OH + NO \rightarrow HCHO + HNO \quad (9a)$$

Pagsberg et al. report a rate coefficient of 2.5×10^{-11} cm^3 molecule^{-1} s^{-1}; however, slightly higher values are necessary to obtain a good fit to our complete data set ($(3.5-5.5) \times 10^{-11}$ cm^3 molecule^{-1} s^{-1}).

No data is available for the reaction of the α,δ-dihydroxyalkenes radicals with NO. They were assumed to react at the same rate as CH_2OH:

$$\alpha,\delta\text{-}(OH)_2C_5H_7 + NO \rightarrow \text{products} \quad (9b)$$

Another likely NO termination process is the depletion of hydroxyl-alkeneoxydes by NO. To explore this option, an isomer-independent depletion step of the alkeneoxides was implemented in the model:

$$\beta,\delta\text{-}OHC_5H_8O + NO \rightarrow \text{products} \quad (10)$$

Although it is known that most alkan- and alkenoxydes react quickly with NO,[45] no data was found for C_5-oxides. Lotz and Zellner[50] measured a value of 3.9×10^{-11} cm^3 molecule^{-1} s^{-1} for 2-butoxy, quite close to the proposed value for k_9. Therefore, assuming the true value to be similar to Lotz and Zellner's, the same starting value for k_{10} as for k_9 was used (2.5×10^{-11} cm^3 molecule^{-1} s^{-1}), and both values were initially varied together. Once a stable fit was achieved, both rates were varied independently. A good fit of the data was achieved at rates of $(4-5) \times 10^{-11}$ cm^3 molecule^{-1} s^{-1} for k_{10}, very close to the one determined for butoxy.

Simulation Approach and Results. In this work, we report the observation of temporal profiles of a single radical species. Given the complexity of the oxidation process and the entwined nature of the oxygen and NO reactions, it is difficult to find conditions in which one species becomes rate determining. Therefore, we focused on our ability to reproduce our experimental data under all conditions with the MCM reaction subset described above, using solely the added reactions R5 and R9 + R10 as adjustable parameters. Afterward, we undertook an extended sensitivity analysis to determine the extent to which the rate coefficients in the MCM can be constrained by our observations.

Simulations were performed independently for all three isotopic variants. We were able to achieve a good match of all experimental data sets for R1, R2, and R3 using similar values for k_5 ($>7 \times 10^{-12}$ cm^3 molecule^{-1} s^{-1}) and k_9 and k_{10} ($\sim 4 \times 10^{-11}$ and 5×10^{-11} cm^3 molecule^{-1} s^{-1}, respectively). Detailed values for each reaction for this set of simulations can be found in Table 4 ("standard model").

The results of the simulations together with the experimental data are shown in Figures 4, 5, and 6 for reactions R1, R2, and R3, respectively. The first noticeable feature of the experimental data is that the sensitivity of the OH/OD regeneration decreases with increasing oxygen partial pressure. This becomes especially pronounced above 1 Torr of oxygen and for the low isoprene/high NO cases (Figures 4b, 5b, and 6b) reaches the point where it stops being rate-determining. (Figures 4a and 6a are the exceptions to this behavior.) This is nicely reproduced by the simulations and is a stable feature of them over a wide range of possible rate coefficients. This in turn constrains greatly our ability to match the data because simulating a higher rate of OH/OD regeneration for high O_2 invariably will also significantly alter the spread and spacing between OH profiles at lower O_2 mixing ratios. Therefore, the matching process tried to balance both spacing and maximum O_2 regeneration values.

In the chosen set of simulations, we see that, in general, for the three data sets where OH steady states are reached within the recorded time frame a very good match is achieved, regardless of isotopomer and varying isoprene/NO ratios. However, the maximum O_2 profiles are in some cases slightly too low, mostly because simulations predict a faster approach

TABLE 4: Simulation Results

	k_6 [10^{-12} cm^3 molecule^{-1} s^{-1}]	k_5 [10^{-12} cm^3 molecule^{-1} s^{-1}]	k_9 [10^{-11} cm^3 molecule^{-1} s^{-1}]	k_{10} [10^{-11} cm^3 molecule^{-1} s^{-1}]
reaction	OH + C_5H_8			
reference model	8.0	7.0−200	4.0	5.0
best possible fit	10	4.0−200	3.5	4.0
Reitz et al.'s parameters	25	3.0		3
reaction	OH + C_5D_8			
reference model	8.0	6.5−200	4.0	4.5
best possible fit	10	3.5−200	4.0	4.5
Reitz et al's parameters[a]	25	3.0		3
reaction	OD + C_5H_8			
reference model	8.0	7.0−200	3.5	4.5
best possible fit	10	4.0−200	4.0	5.5
Reitz et al.'s parameters[a]	25	3.0		3

[a] As shown in Figure 9, it was not possible to achieve a good match of our experimental data and simulations using these rate coefficients.

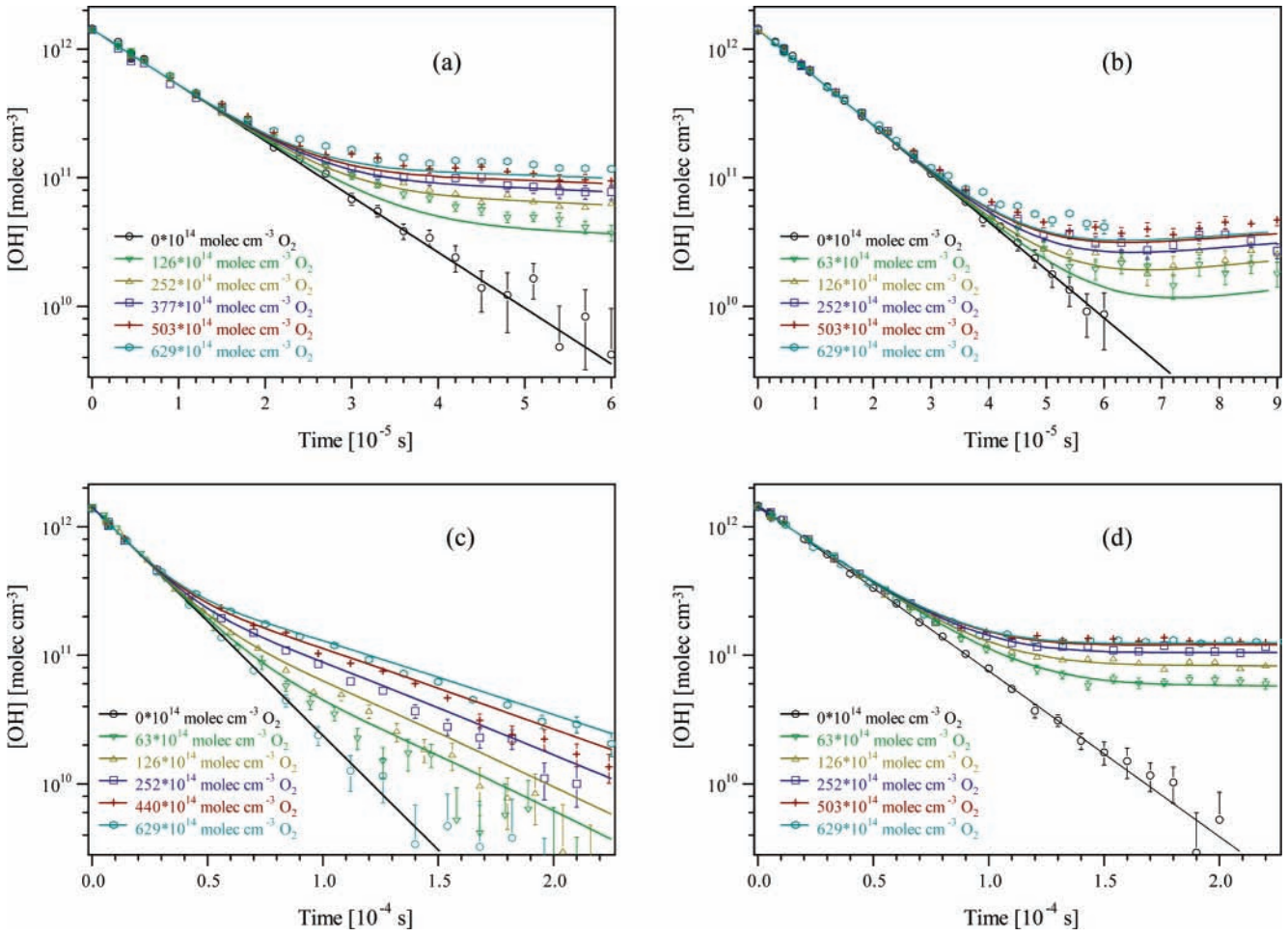

Figure 4. OH + h_8-C_5H_8 (reference model, k_6 lit.): (a) $k_6 = 8 \times 10^{-12}$, (b) $k_5 = 7 \times 10^{-12}$, (c) $k_9 = 4.0 \times 10^{-11}$, and (d) $k_{10} = 5.0 \times 10^{-11}$ cm^3 molecule^{-1} s^{-1}.

to oxygen-independent conditions than observed experimentally. This is quite apparent for parts a and b of Figure 5, which also contain the data with the highest relative error. It will be shown below that hydroxyalkyl formation can resolve this discrepancy; however, it should be noted that these discrepancies are within the range of the NO concentration errors reported in Table 3.

This suggests that the Leeds MCM is able to reproduce the temporal profiles of a key intermediate, HO_2, with reasonable accuracy for a wide range of experimental conditions. The ability to match the temporal profiles for the three isotopomeric variants of R1 with a single mechanism gives us added confidence in the robustness of these results. In a subsequent discussion, we will refer to these model results, with Atkinson's value for k_6 and just one NO termination step, as the standard model.

Sensitivity Analysis. Figure 7 shows simulations of the temporal profiles of a number of reactive intermediates for each set of isoprene/NO ratios for R1 at the highest O_2 concentration using the standard model. As expected, the achievement of an OH steady state is mirrored by the buildup of an HO_2 steady state in the same time frame. In cases a and d, this happens so rapidly that our simulations are mainly sensitive to the end steady state and hence to the ratio of the overall speed of HO_2 formation versus the reaction with isoprene. In case b, the OH profiles are more sensitive to the speed of the initial HO_2 buildup

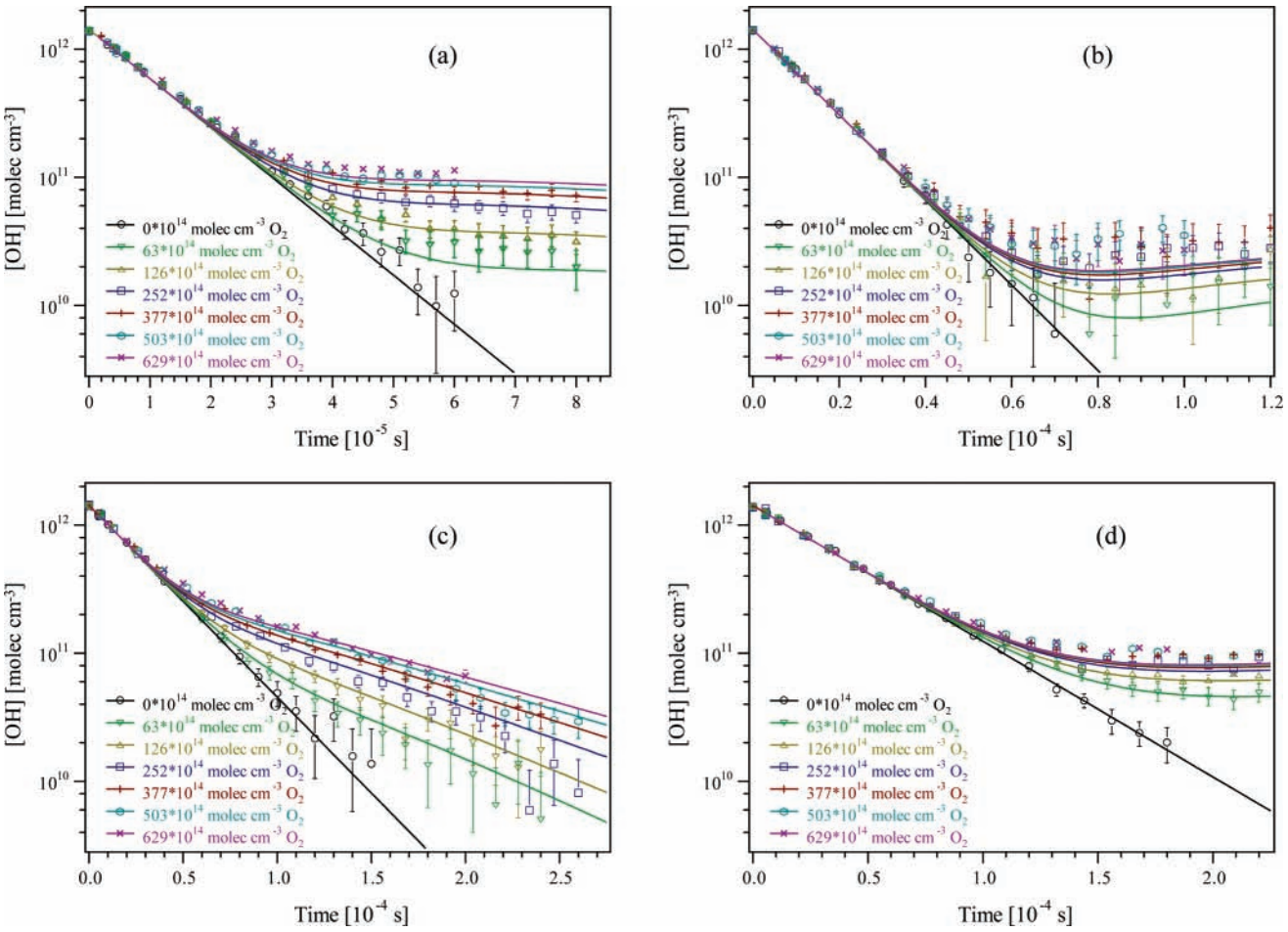

Figure 5. OD + h_8-C_5H_8 data and simulation results (reference model, k_6 lit.): (a) $k_9 = 8 \times 10^{-12}$, (b) $k_5 = 7 \times 10^{-12}$, (c) $k_9 = 4.0 \times 10^{-11}$, and (d) $k_{10} = 4.5 \times 10^{-11}$ cm^3 molecule^{-1} s^{-1}.

so that small variations in k_6, k_7, and k_9 can have a large impact. In case c, however, no steady state is reached because of NO termination reactions. The OH simulations for this case are sensitive to variations in k_9 and k_{10}, the reactions that directly reduce HO_2 and hence recycled OH available to the system.

Hydroxyalkeneperoxy Formation (R5). In the standard model, k_5 stops being rate-determining for our system for values above 8×10^{-12} cm^3 molecule^{-1} s^{-1} for all isotopic variants, and a good fit of the data can still be achieved down to 7×10^{-12} (R1), the exact lower limit being dependent on the choices for k_9 and k_{10} (which are kept at the lowest possible values). Values below 7×10^{-12} cm^3 molecule^{-1} s^{-1} can be reconciled with the data only if subsequent steps are accelerated. As discussed below, the fragmentation/rearrangement step (R7) is not rate-determining and cannot be accelerated further. The rate coefficients for R8 and R4 are fairly well established, so both were accelerated by only 20% for test purposes. Whereas the variation of k_8 does not change the simulation results, speeding up the rate of OH regeneration (R4) does have a significant impact on the simulation output, which can be offset by slowing down k_5 to about 5×10^{-12} cm^3 molecule^{-1} s^{-1}.

The other reaction that has a strong impact on the simulation results is the formation of alkenoxides (R6). Speeding up this reaction has a direct effect on the lower limit of k_5, and possible values of k_6 will be discussed in detail in the next section. Using a rate coefficient of $\sim 12 \times 10^{-12}$ cm^3 molecule^{-1} s^{-1}, the fastest rate coefficient consistent with our data, the lower limit of k_5 is around 2×10^{-12} cm^3 molecule^{-1} s^{-1}.

Hydroxyalkeneoxy Formation (R6). The value of 8×10^{-12} cm^3 molecule^{-1} s^{-1} for k_6 proposed by Atkinson and used in our standard model has been widely accepted as a good estimate for most dienes. The original version of the MCM[18] proposed a lower value of 3.9×10^{-12} cm^3 molecule^{-1} s^{-1} based on an assumed size dependency that has been discarded since.[36] However, in a recent paper on cycling experiments similar to this work by Reitz et al.,[23] it has been suggested that k_6 could be as fast as 2.5×10^{-11} cm^3 molecule^{-1} s^{-1}. Because the value of k_6 has a strong impact on our determination of k_5, a detailed sensitivity analysis was performed.

As can be seen in the plot of the reaction intermediates in Figure 7, simulations a, b, and d are mechanistically similar and differ only in the time gap between the alkeneperoxide and HO_2 production, case a being the fastest and b being the one with the slowest conversion rate. Given that the rate coefficient for HO_2 production from CH_2OH is a fixed parameter, this conversion rate is solely dependent on the alkenoxy-formation/degradation. Therefore, data set b should be the most sensitive to reactions R6 and R7.

As stated before, Figures 4b, 5b, and 6b show that, although still within the error limits of the measurements, the simulation results are systematically too low. It is possible to achieve a closer match by either increasing k_6 or k_7. However, as discussed in detail below, at the rates used in the MCM, unimolecular step R7 is non-rate-determining under the conditions of our experiments so that faster HO_2 formation can be accomplished solely by increasing the rate of hydroxy-alkeneoxyde formation

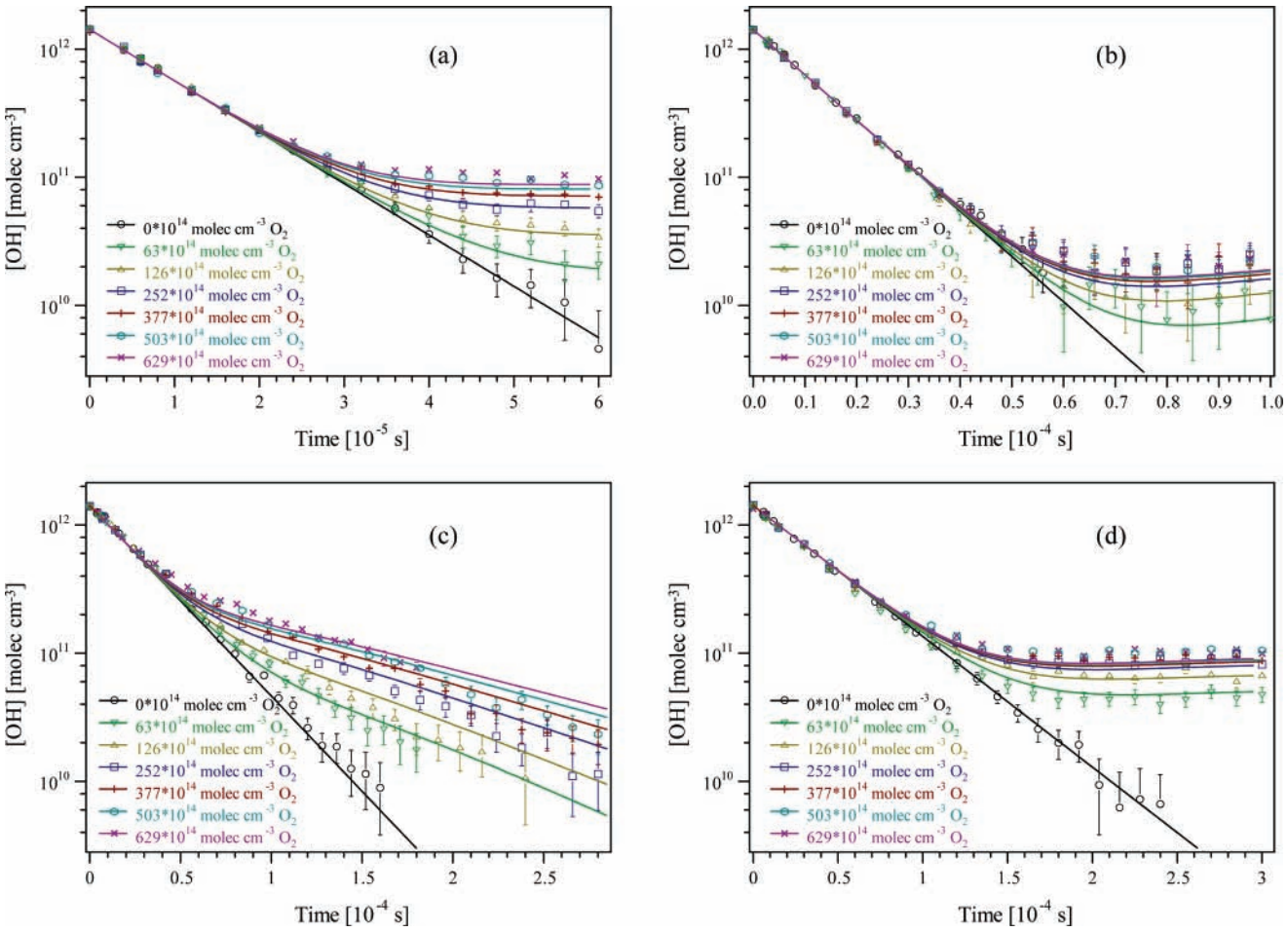

Figure 6. OH + d_8-C_5H_8 data and simulation results (reference model, k_6 lit.): (a) $k_6 = 8 \times 10^{-12}$, (b) $k_5 = 7 \times 10^{-12}$, (c) $k_9 = 3.5 \times 10^{-11}$, and (d) $k_{10} = 4.5 \times 10^{-11}$ cm^3 molecule^{-1} s^{-1}.

(k_6). By increasing k_6 by 20%, we can indeed achieve an almost perfect match of simulation and experimental points as shown in Figure 8. This is also true for the systems OD + C_5H_8 and OH + C_5D_8 (cf. Table 4, "best fit"). If k_6 is increased by more than 50% over the MCM value, then it is not possible to simulate our experimental profiles.

Hydroxyalkeneoxy Fragmentation/Rearrangement (R7). In the MCM as well as in our reference model, k_7 was made fast enough to be non-rate-determining under normal conditions, with values of 1×10^6 s^{-1} for the fragmentation and 6×10^5 s^{-1} for the rearrangement. To explore the lower limit of k_7, we reduced both channels by the same amount. Using the reference model, we found that the lower limit in our system lies about 50% lower than the initial values, and if the best-fit scenario described above is used, a reduction by 70% is feasible. Therefore, the "lowest limit" values for k_7 that are consistent with our data are $(1.5-5) \times 10^5$ s^{-1} for k_{7a} and 1×10^5 s^{-1} for k_{7b}.

HO_2 Production (R8). As already mentioned before, small changes in the value of k_8 have little impact on the first steps of the oxidation mechanism. However, whereas k_{8b} (HO_2 formation from CH_2OH) is a well-characterized reaction coefficient, the value for k_{8a}, analogous HO_2 formation from the α,δ-dihydroxyalkene, is fairly speculative. Because the yield of the dihydroxyalkenes is fairly low in the MCM, the impact of our assumption on the value of k_{8a} is minor. To quantify that impact, we set $k_{8a} = 0$ (i.e., no OH regeneration from the products of the δ-hydroxyperoxides). To match the data, higher peroxide-formation rates k_5 have to be used, around 1.5×10^{-11} cm^3 molecule^{-1} s^{-1}, and smaller values for k_9 and k_{10} are feasible, $\sim 2 \times 10^{-11}$ cm^3 molecule^{-1} s^{-1} (cf. below), although the data match is significantly worse than in standard model, as in all simulations where we tried to introduce larger channel asymmetries. Given the overall complexity of the mechanism, this is no proof of a symmetric mechanism. However, it is very unlikely that no HO_2 formation comes from this still very poorly understood part of the isoprene oxidation scheme, suggesting that the implied maximum uncertainty of 10 in the minimum value for k_5 ($(1.5-15) \times 10^{-12}$ cm^3 molecule^{-1} s^{-1}) is on the conservative side.

NO Termination Steps. At the higher NO levels, the reference model is very sensitive for the values of k_9 and k_{10}. The data sets at high NO and low isoprene concentrations (case c) constrain the lower limit ($\sim 6 \times 10^{-11}$ cm^3 molecule^{-1} s^{-1}) almost independently of the choices for k_4, k_5, or k_6, whereas on the high end values up to 1×10^{-10} cm^3 molecule^{-1} s^{-1} can be reconciled with the data (cases a and d) by lowering k_5 or k_6. Values of 4×10^{-11} and 5×10^{-11} cm^3 molecule^{-1} s^{-1} used in the reference model were chosen because they gave the best match at the closest values to the literature values from Pagsberg et al. (2.5×10^{-11} cm^3 molecule^{-1} s^{-1}) as well as Lotz and Zellner (3.9×10^{-11} cm^3 molecule^{-1} s^{-1}). It should be noted, however, that without the data sets of case c, a match of the other data is possible with values for both k_9 and k_{10} around 2×10^{-11} cm^3 molecule^{-1} s^{-1}, very close to the literature

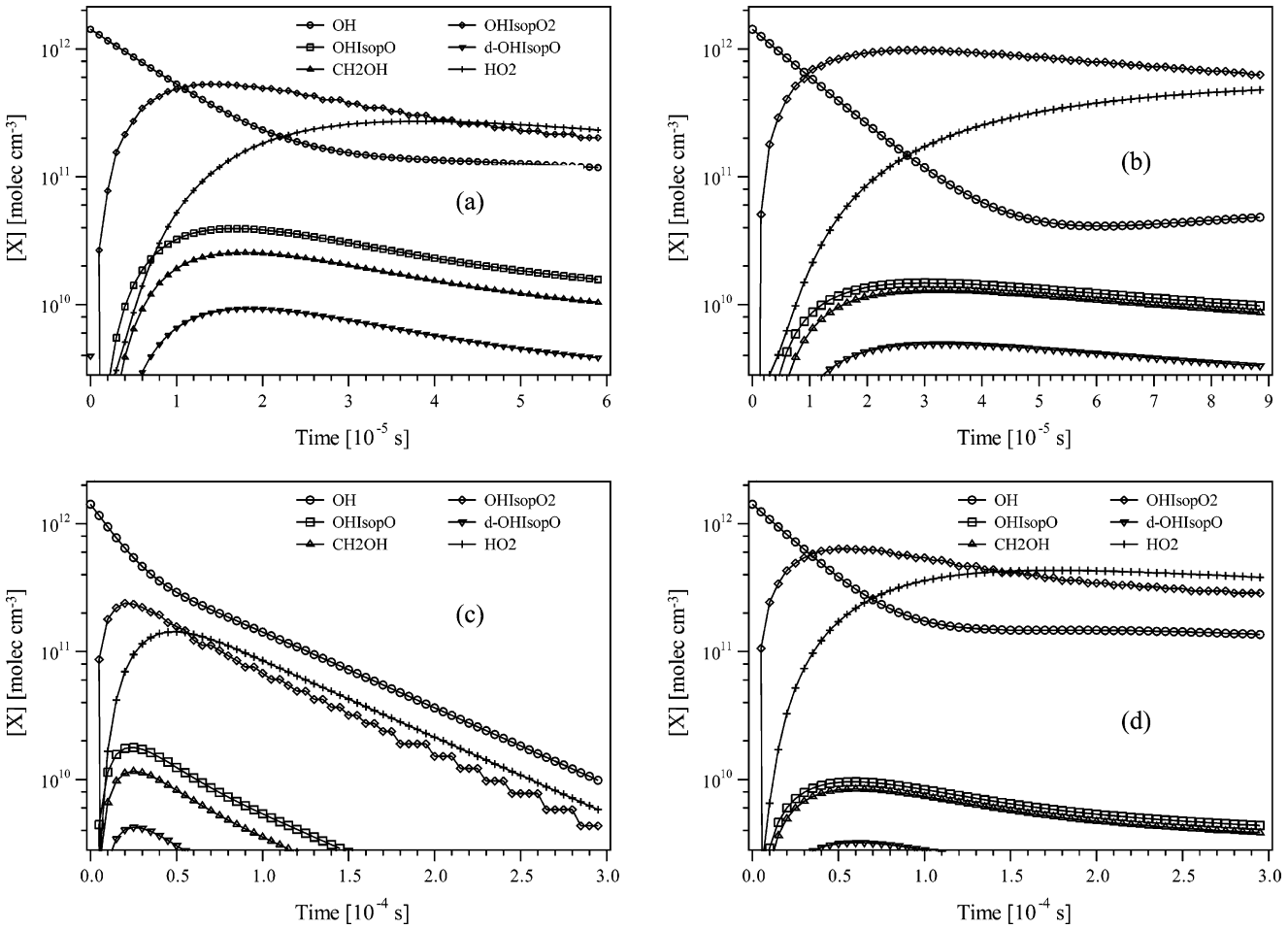

Figure 7. OH + h_8-C_5H_8 data and simulation results (reference model, k_6 lit.): peroxi, alkoxy, and HO_2 production.

considering our NO concentration uncertainty and the uncertainties in the work of Pagsberg et al.

Besides the NO termination steps included in our model, a reduction of the final HO_2 yield in the presence of high NO concentrations can also be accomplished by increasing the branching ratio for the formation of hydroxyalkenenitrates (k_{5b}). The MCM mechanism uses an average nitrate yield of ~10% from the reaction of hydroxy-peroxides with NO. To explore the sensitivity of our simulations to this branching ratio, an isomer-independent linear increase of the alkenenitrate yield was implemented in the model. By increasing the MCM yields by a factor of 2, giving 14 to 22% total alkenenitrate yields depending on the channel, k_9 and k_{10} could be reduced to ~2.5 $\times$ 10^{-11} cm^3 molecule^{-1} s^{-1} while still describing the experimental data adequately. However, such a large nitrate yield is not consistent with prior data. Because we are not able to differentiate between the various NO loss processes, the uncertainties in k_9 and k_{10} preclude us from constraining the nitrate yield further.

Finally, it should be stressed again that these high values for k_9, k_{10}, and/or k_{5b} are mainly required to fit one set of data (high NO, low isoprene) that is the one farthest from any previous smog chamber or field study.

Simulation Discussion. *Dependence on Isotopomers.* All current mechanisms assume that for all OH additions to alkenes the hydrogen being abstracted from CH_2OH and the γ-hydroxyalkencarbonyl radicals come from the OH. If main-chain hydrogens are observed in HO_2 formation, this would be an indication of either special rearrangements of the alkenoxy intermediates and/or an OH abstraction path. Within experimental error, we obtain identical rate coefficients for three of the isotopomeric variants of R1, suggesting that OH abstraction plays no significant role. The ability of LIF detection to monitor both OH and OD simultaneously allows us to observe the extent of any reaction proceeding via abstraction or rearrangement. As a direct test, the OD signal in the OH cycling of reaction 3 and the OH signal in the OD cycling of reaction 2 were monitored. In the first case, no OD signal was detected; in the latter, OH at about 5% of the OD signal was measured. This was consistent with the level of isotopic impurities of the OD precursor (DNO_3), so significant OH regeneration from the cycling process itself can be ruled out in our experiments.

These experiments suggest that neither abstraction nor rearrangement is significant under our experimental conditions. As noted above, all isomeric variants of the reaction mechanism were simulated with the same mechanism, further suggesting that none of the steps that are rate-determining in cycling OH have an isotopic dependence, that is, peroxide formation (k_5), oxide formation (k_6), and NO termination steps (k_9 and k_{10}).

However, it is conceivable that the rearrangement reactions (k_{7b}), involving an H shift, show an isotopic effect that cannot be seen under our experimental conditions but could play a role in chamber studies with lower NO mixing ratios.

Formation of Hydroxyalkeneperoxides. For peroxiradical formation, a value of at least 7×10^{-12} cm^3 molecule^{-1} s^{-1} for k_5 is needed for a good match of the data with the simulations, dropping to 4×10^{-12} cm^3 molecule^{-1} s^{-1} if higher values for k_6 are used. These values are within the range that past and current recommendations have been proposing for this step, (8−28) $\times$ 10^{-13} cm^3 molecule^{-1} s^{-1} for most alkenes.[51] There have

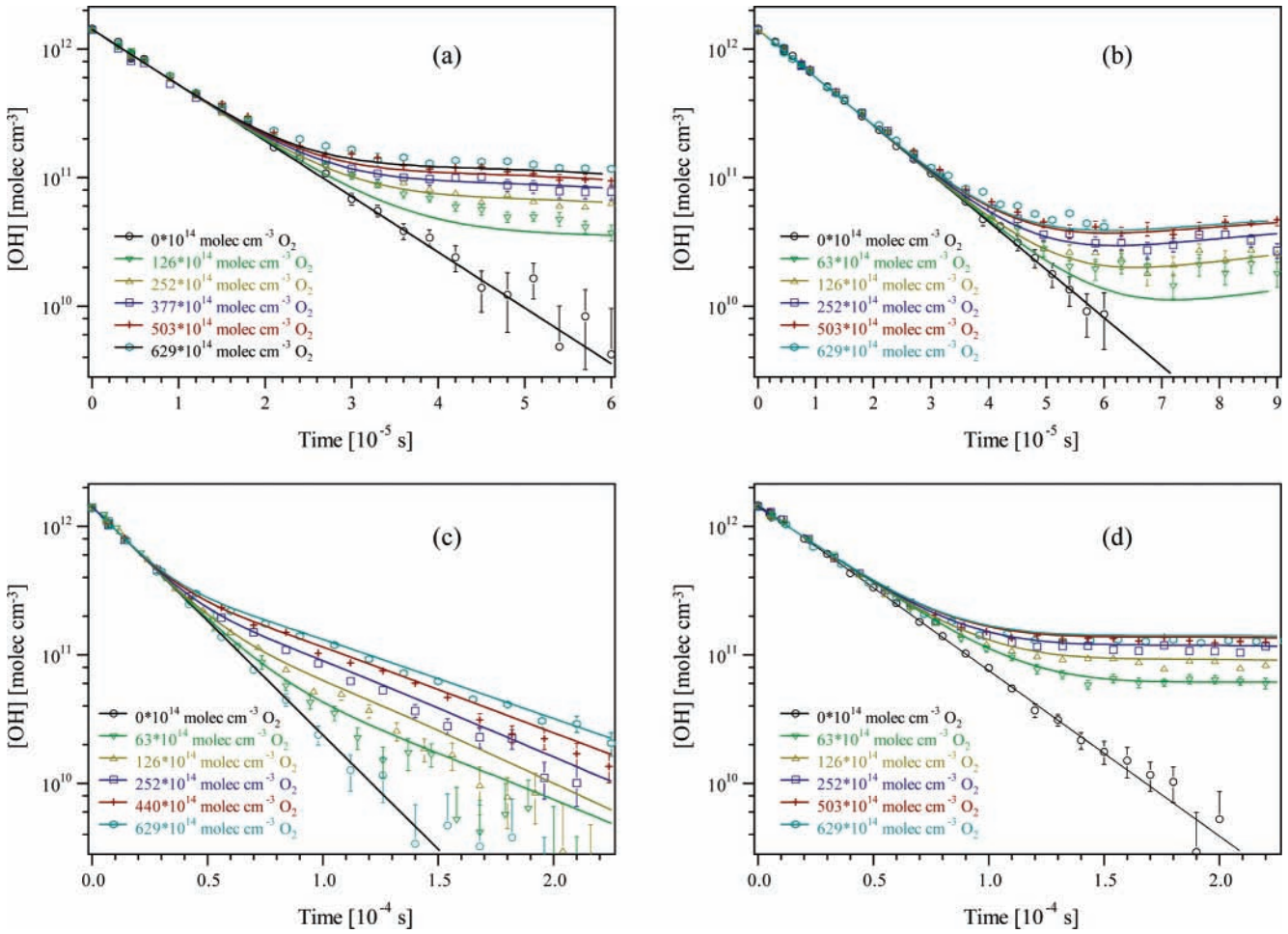

Figure 8. OH + h_8-C_5H_8 data and simulation results (best possible fit): (a) $k_6 = 10 \times 10^{-12}$, (b) $k_5 = 4 \times 10^{-12}$, (c) $k_9 = 3.5 \times 10^{-11}$, and (d) $k_{10} = 4.0 \times 10^{-11}$ cm^3 molecule^{-1} s^{-1}.

recently been two attempts by Zhang and co-workers to directly measure the formation of the peroxides in a flow tube with CIMS detection of the products: initially they reported[30] a rate of 2.8×10^{-15} cm^3 molecule^{-1} s^{-1}, and later,[27] a value of 7×10^{-13} cm^3 molecule^{-1} s^{-1}. The latter is closer to the results from CTST calculations from the same group,[28] namely, a range of $(1-10) \times 10^{-13}$ cm^3 molecule^{-1} s^{-1}. All of these rates are significantly too slow to be consistent with our data, even assuming a much faster rate for the alkenoxy formation (cf. Figure 9 and our sensitivity analysis). Recent results from the same group using a similar OH cycling approach to that presented here,[23] however, use a much higher rate, 3×10^{-12} cm^3 molecule^{-1} s^{-1}. Two other previous determinations via OH cycling, however, used 2×10^{-12} cm^3 molecule^{-1} s^{-1} (Siese et al.[52]) and 6.9×10^{-12} cm^3 molecule^{-1} s^{-1} (Stevens et al.[41]). Recently, in a new set of OH cycling experiments, Chuong and Stevens[26] proposed a very fast rate, 2.8×10^{-11} cm^3 molecule^{-1} s^{-1}. The rate coefficient obtained here is consistent with the results from Stevens and co-workers. Table 5 summarizes the experimental conditions and elementary rate coefficients obtained in OH cycling studies. Without a detailed description of the models used, it is difficult to determine if these differences simply reflect a different choice in the elementary rates and mechanism. However, we note and discuss in more detail below that the effect of NO termination steps in influencing derived rates must be considered. These reactions are unimportant in the atmosphere and, as a consequence, the experimental database is either poor or nonexistent, and this limits the ability of recycling studies to constrain elementary rates.

Formation of Hydroxyalkeneoxydes (k_6). As discussed above, the alkenoxy radical formation is fairly constrained in our simulations between 8×10^{-12} and 12×10^{-12} cm^3 molecule^{-1} s^{-1}. In 1992, the IUPAC panel proposed 8×10^{-12} cm^3 molecule^{-1} s^{-1} for the generic RO_2 + NO step for small alkenes;[53] however, in the initial protocol paper for the MCM,[18] a lower value, 3.8×10^{-12}, was proposed on the basis of structural additivity reasoning that has been abandoned since (cf. the latest MCM protocol paper[36] and Eberhard and Howard[54]) so that the current MCM again uses 8×10^{-12} cm^3 molecule^{-1} s^{-1}, in excellent agreement with this work. The two aforementioned cycling studies by Stevens and co-workers[26,41] are consistent with our results, reporting rates of 9×10^{-12} (1999) and 11×10^{-12} cm^3 molecule^{-1} s^{-1} (2002) for k_6, albeit with a higher nitrate branching ratio. In contrast to this, Reitz et al.[23] proposes a value for k_6 of 2.5×10^{-11} cm^3 molecule^{-1} s^{-1}, which is 3 times faster, to interpret their OH cycling experiments. As noted in the mechanism description, k_6 values are heavily dependent on the choice of k_7, the fragmentation step, for which Reitz et al. uses an exceptionally low value of 3×10^4 s^{-1}. We ran simulations with k_6 set at 2.5×10^{-11} cm^3 molecule^{-1} s^{-1} and varied k_5 and k_7; however, as shown in Figure 9, it was not possible to achieve a good match of our experimental data under these conditions.

Fragmentation/Rearrangement of the Hydroxyalkeneoxydes (k_7). As already mentioned in the model description, there are no direct measurements of these unimolecular steps, and the values used here, around 1×10^6 s^{-1}, are within the mainstream of estimates. Recently, in the OH cycling studies

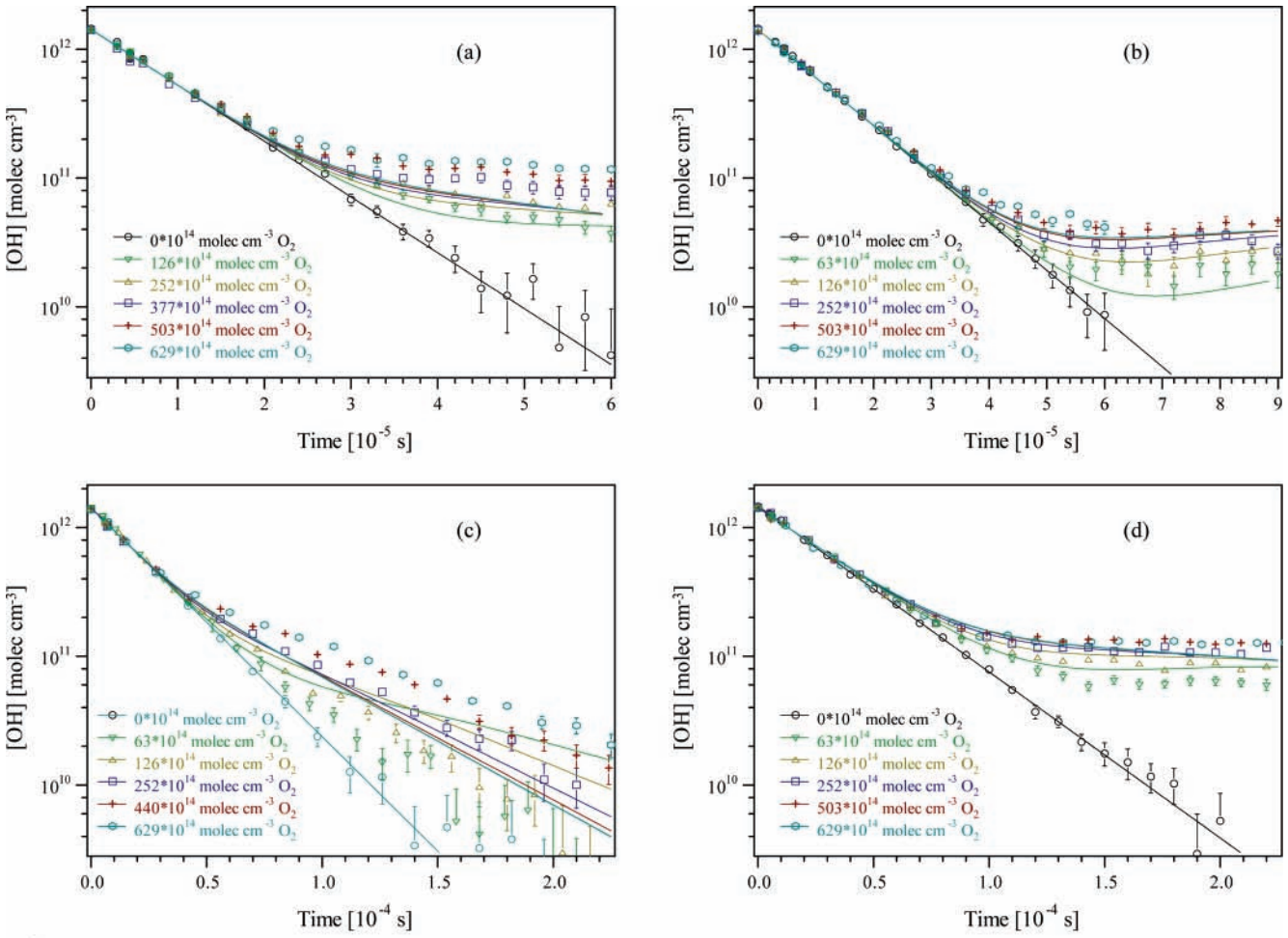

Figure 9. OH + h_8-C_5H_8 data and simulation results (Reitz et al.'s parameters): $k_6 = 25 \times 10^{-12}$, $k_5 = 3 \times 10^{-12}$, $k_{10} = 3 \times 10^{-11}$ cm^3 molecule^{-1} s^{-1}.

TABLE 5: Comparison of Experimental and Simulation Parameters in Recent OH/Isoprene Cycling Studies

	this work	Stevens et al. 1999[41]	Choung and Stevens 2002[26]	Reitz et al. 2002[23]
pressure [Torr]	200 [N_2]	2 [He]	100−150 [Ar]	3−4 [He]
isoprene [10^{11} molecules cm^{-3}]	2000−10 000	3−20	3−18	1000−3000
NO [10^{12} molecules cm^{-3}]	7−600	10−20	7−42	0−3600
O_2 [10^{15} molecule cm^{-3}]	2−20	2−8	5−16	30
OH detection	PLP/PLIF	DF/LIF	TFT /LIF	PLP/PLIF
k_1 [10^{11} molecule^{-1} s^{-1} cm^3]	8.47	11	10.8	10
k_5 [10^{12} molecule^{-1} s^{-1} cm^3]	4−200	6.9	0.3−28	3
k_{6a} [10^{12} molecule^{-1} s^{-1} cm^3]	8−12	9	11	25
k_{6b} (avg % of k_{5a})	10		15	0
k_7 [10^5 s^{-1}]	>2.5	1.5	1.5	0.3
k_9 [10^{11} molecule^{-1} s^{-1} cm^3]	3.5	not included	not included	not included
k_{10} [10^{11} molecule^{-1} s^{-1} cm^3]	4.5	not included	not included	3

discussed above, lower values for k_7 were proposed: Stevens and co-workers use a value of 1.5×10^5 s^{-1} in both of their studies; Reitz et al., as already mentioned, proposed a rate coefficient for the fragmentation step in 2 Torr of He of 3×10^4 s^{-1}. To explain this very low value for k_{7a}, they argue that the fragmentation step is still in the falloff region at that low pressure.

By design, OH cycling experiments are not really sensitive to this step because it cannot be explored by concentration changes, and the other alternative, varying the total reaction time, is limited by detection issues. The two studies by Stevens and co-workers were conducted at 2 and 150 Torr and used similar values for k_{7a}. These values are fairly close to the lower limit we found in this study, although they use substantially lower NO concentrations and their chemical model does not appear to include reactions 9, 10, or 7b. The use of a rate coefficient that is substantially lower than current recommendations, without any additional evidence that k_{7a} is indeed in the falloff region, appears rather speculative.

Formation of Hydroxyalkenenitrates (k_{5b}). Our reference model uses an average nitrate yield of 10% from the reaction of hydroxy-peroxides with NO. This agrees well with the measurements from Tuazon and Atkinson and Sprengnether et al.[15,55] Recently, in Choung and Stevens cycling study[26] a higher branching ratio of 15% was suggested. However, Chen et al.

found a yield of 5% by direct detection of the nitrates in a chamber experiment.[56]

Again, our sensitivity toward this step is limited by the large uncertainties in the other NO-induced termination steps. In Choung and Stevens' experiments, they were able to find conditions where their sensitivity for this step was considerable; however, they did not include any other NO termination steps. We calculate that at the conditions they undertook their nitrate yield determination k_9 and k_{10} should have had an impact of equal magnitude had it been included in their model. Our results suggest that uncertainties in k_9 and k_{10} preclude constraints on nitrate yields from OH cycling experiments and that direct determinations of k_9 and k_{10} are needed to assess the validity of Choung and Stevens' yields.

NO Termination Steps (k_9, k_{10}). The largest uncertainty in the proposed mechanism lies in the values for these steps. These reactions are not atmospherically relevant because they cannot compete with reactions R7a and 8 under typical atmospheric conditions. Consequently, they have received little attention. In fact, even the data from most chamber studies would not be affected significantly by the values for k_9 and k_{10} that we propose here.[15] However, because CH_2OH is the main fragmentation product in any atmospheric oxidation scheme of alkenes, future OH cycling studies would greatly benefit from a direct determination of at least k_9, the experimentally more accessible reaction.

Conclusions

The ultraviolet absorption spectrum of h_8-isoprene and d_8-isoprene in the range of 200−240 nm has been measured with high absolute precision. On the basis of the absorption cross sections from this new data set, the kinetic data from our previous investigation of the OH/isoprene reaction was reanalyzed. We obtain a rate coefficient for R1, R2, and R3 that is 15% lower than current recommendations at room temperature but with a temperature dependence over the range of 250−350 K in agreement with two previous studies. A conservative analysis of the accuracy and precision of the data suggests that the uncertainty in our results should be ±5% unless we have a significant unknown systematic error.

The isoprene module of the current version of the University of Leeds' master chemical mechanism was able to predict the HO_2/DO_2 regeneration rates observed experimentally in the systems OH/h_8-isoprene, OH/d_8-isoprene, and OD/h_8-isoprene over a wide range of nitric oxide, oxygen, and isoprene concentrations. This suggests that the rates and mechanism of the major oxidation pathways of isoprene are accurately represented in the MCM. Through a detailed sensitivity analysis, we have also shown that OH cycling is a useful independent experimental technique for testing and formulating constrains on a complex mechanism such as isoprene oxidation. However, regardless of experimental precision or concentration range, the uncertainties in the nitric oxide termination steps significantly limit the ability of such cycling experiments to constrain individual steps such as nitrate yield better.

Acknowledgment. We thank Cheryl Tatum for assistance with the isoprene cross-section measurements. We thank Roger Atkinson and Phil Stevens for helpful conversations. This work was supported by the National Science Foundation through grant ATM0002242.

Supporting Information Available: Values of the UV absorption cross sections of h_8- and d_8-isoprene, the mechanism of the OH + CH_4 simulation, and the condensed mechanism of isoprene photooxidation together with the results of the methane simulations. This material is available free of charge via the Internet at http://pubs.acs.org.

References and Notes

(1) Guenther, A.; Hewitt, C. N.; Erickson, D.; Fall, R.; Geron, C.; Graedel, T.; Harley, P.; Klinger, L.; Lerdau, M.; McKay, W. A.; Pierce, T.; Scholes, B.; Steinbrecher, R.; Tallamraju, R.; Taylor, J.; Zimmerman, P. *J. Geophys. Res.* **1995**, *100*, 8873.

(2) Keller, M.; Lerdau, M. *Global Biogeochem. Cycles* **1999**, *13*, 19.

(3) Bonsang, B.; Polle, C.; Lambert, G. *Geophys. Res. Lett.* **1992**, *19*, 1129.

(4) Milne, P. J.; Riemer, D. D.; Zika, R. G.; Brand, L. E. *Mar. Chem.* **1995**, *48*, 237.

(5) Yokouchi, Y.; Li, H.-J.; Machida, T.; Aoki, S.; Akimoto, H. *J. Geophys. Res.* **1999**, *104*, 8067.

(6) Singh, H. B.; Gregory, G. L.; Anderson, B.; Browell, E.; Sachse, G. W.; Davis, D. D.; Crawford, J.; Bradshaw, J. D.; Talbot, R. W.; Blake, D. R.; Thornton, D.; Newell, R.; Merill, J. T. *J. Geophys. Res.* **1996**, *101*, 1907.

(7) Maurezall, D. L.; Jacob, D. J.; Fann, S.-M.; Bradshaw, J. D.; Gregory, G. L.; Sachse, G. W.; Blake, D. R. *J. Geophys. Res.* **1996**, *101*, 4175.

(8) Hauglustaine, D. A.; Madronich, S.; Ridley, B. A.; Flocke, S. J.; Cantrell, C. A.; Eisele, F. L.; Shetter, R. E.; Tanner, D. J.; Ginoux, P.; Atlas, E. L. *J. Geophys. Res., [Atmos.]* **1999**, *104*, 30275.

(9) Pierce, T.; Geron, C.; Bender, L.; Dennis, R.; Tonnesen, G.; Guenther, A. *J. Geophys. Res., [Atmos.]* **1998**, *103*, 25611.

(10) Fuentes, J. D.; Lerdau, M.; Atkinson, R.; Baldocchi, D.; Bottenheim, J. W.; Ciccioli, P.; Lamb, B.; Geron, C.; Gu, L.; Guenther, A.; Sharkey, T. D.; Stockwell, W. *Bull. Am. Meteorol. Soc.* **2000**, *81*, 1537.

(11) Poisson, N.; Kanakidou, M.; Crutzen, P. J. *J. Atmos. Chem.* **2000**, *36*, 157.

(12) Atkinson, R.; Aschmann, S. M.; Winer, A. M.; Pitts, J. N., Jr. *Int. J. Chem. Kinet.* **1982**, *14*, 507.

(13) Benkelberg, H. J.; Boge, O.; Seuwen, R.; Warneck, P. *Phys. Chem. Chem. Phys.* **2000**, *2*, 4029.

(14) Jenkin, M. E.; Boyd, A. A.; Lesclaux, R. *J. Atmos. Chem.* **1998**, *29*, 267.

(15) Sprengnether, M.; Demerjian, K. L.; Donahue, N. M.; Anderson, J. G. *J. Geophys. Res., [Atmos.]* **2002**, *107*, 10.1029/2001JD000716

(16) Ruppert, L.; Becker, K. H. *Atmos. Environ.* **2000**, *34*, 1529.

(17) Carter, W. P. L.; Pierce, J. A.; Luo, D. M.; Malkina, I. L. *Atmos. Environ.* **1995**, *29*, 2499.

(18) Jenkin, M. E.; Saunders: S. M.; Pilling, M. J. *Atmos. Environ.* **1997**, *31*, 81.

(19) Paulson, S. E.; Flagan, R. C.; Seinfeld, J. H. *Int. J. Chem. Kinet.* **1992**, *24*, 79.

(20) Carter, W. P. L.; Atkinson, R. *Int. J. Chem. Kinet.* **1996**, *28*, 497.

(21) Campuzano-Jost, P.; Williams, M. B.; D'Ottone, L.; Hynes, A. J. *Geophys. Res. Lett.* **2000**, *27*, 693.

(22) Zhang, D.; Zhang, R. Y.; Park, J.; North, S. W. *J. Am. Chem. Soc.* **2002**, *124*, 9600.

(23) Reitz, J. E.; McGivern, W. S.; Church, M. C.; Wilson, M. D.; North, S. W. *Int. J. Chem. Kinet.* **2002**, *34*, 255.

(24) Gill, K. J.; Hites, R. A. *J. Phys. Chem. A* **2002**, *106*, 2538.

(25) Dibble, T. S. *J. Phys. Chem. A* **2002**, *106*, 6643.

(26) Chuong, B.; Stevens, P. S. *J. Geophys. Res., [Atmos.]* **2002**, *107*, 10.1029/2001JD000865

(27) Zhang, D.; Zhang, R. Y.; Church, C.; North, S. W. *Chem. Phys. Lett.* **2001**, *343*, 49.

(28) Lei, W. F.; Zhang, R. Y. *J. Phys. Chem. A* **2001**, *105*, 3808.

(29) Zhang, R. Y.; Suh, I.; Lei, W.; Clinkenbeard, A. D.; North, S. W. *J. Geophys. Res., [Atmos.]* **2000**, *105*, 24627.

(30) Zhang, R. Y.; Lei, W. F. *J. Chem. Phys.* **2000**, *113*, 8574.

(31) Stevens, P. S.; Seymour, E.; Li, Z. J. *J. Phys. Chem. A* **2000**, *104*, 5989.

(32) McGivern, W. S.; Suh, I.; Clinkenbeard, A. D.; Zhang, R. Y.; North, S. W. *J. Phys. Chem. A* **2000**, *104*, 6609.

(33) Lei, W. F.; Zhang, R. Y.; McGivern, W. S.; Derecskei-Kovacs, A.; North, S. W. *Chem. Phys. Lett.* **2000**, *326*, 109.

(34) Lei, W. F.; Derecskei-Kovacs, A.; Zhang, R. Y. *J. Chem. Phys.* **2000**, *113*, 5354.

(35) Chuong, B.; Stevens, P. S. *J. Phys. Chem. A* **2000**, *104*, 5230.

(36) Saunders: S. M.; Jenkin, M. E.; Derwent, R. G.; Pilling, M. J. *Atmos. Chem. Phys.* **2003**, *3*, 161.

(37) Silvente, E.; Richter, R. C.; Hynes, A. J. *J. Chem. Soc., Faraday Trans.* **1997**, *93*, 2821.

(38) Jones, L. C.; Taylor, L. W. *Anal. Chem.* **1955**, *27*, 228.
(39) Atkinson, R.; Baulch, D. L.; Cox, R. A.; Hampson, R. F.; Kerr, J. A.; Rossi, M. J.; Troe, J. *J. Phys. Chem. Ref. Data* **1999**, *28*, 191.
(40) Kleindienst, T. E.; Harris, G. W.; Pitts, J. N., Jr. *Environ. Sci. Technol.* **1982**, *16*, 844.
(41) Stevens, P.; L'Esperance, D.; Chuong, B.; Martin, G. *Int. J. Chem. Kinet.* **1999**, *31*, 637.
(42) Atkinson, R. *J. Phys. Chem. Ref. Data* **1997**, 26, 217.
(43) Dibble, T. S. *J. Phys. Chem. A* **1999**, *103*, 8559.
(44) Francisco-Marquez, M.; Alvarez-Idaboy, J. R.; Galano, A.; Vivier-Bunge, A. *Phys. Chem. Chem. Phys.* **2003**, *5*, 1392.
(45) Atkinson, R. *J. Phys. Chem. Ref. Data* **1994**, Monograph No. 2.
(46) Nesbitt, F. L.; Payne, W. A.; Stief, L. J. *J. Phys. Chem.* **1988**, *92*, 4030.
(47) Pagsberg, P.; Munk, J.; Anastasi, C.; Simpson, V. *Chem. Phys. Lett.* **1989**, *157*, 271.
(48) Pagsberg, P.; Munk, J.; Anastasi, C.; Simpson, V. J. *J. Phys. Chem.* **1989**, *93*, 5162.
(49) Pagsberg, P.; Munk, J.; Sillesen, A.; Anastasi, C. *Chem. Phys. Lett.* **1988**, *146*, 375.
(50) Lotz, C.; Zellner, R. *Phys. Chem. Chem. Phys.* **2001**, *3*, 2607.
(51) Atkinson, R.; Baulch, D. L.; Cox, R. A.; Hampson, R. F.; Kerr, J. A.; Rossi, M. J.; Troe, J. *J. Phys. Chem. Ref. Data* **1997**, *26*, 522.
(52) Siese, M.; Koch, R.; Fittschen, C.; Zetzsch, C. Reaction Systems Toluene/O2/NO and Acetylene/O2 and the Addition of OH to Isoprene; Eurotrac Symposium, 1994; Garmisch-Partenkirchen.
(53) Atkinson, R.; Baulch, D. L.; Cox, R. A.; Hampson, R. F.; Kerr, J. A.; Troe, J. *J. Phys. Chem. Ref. Data* **1992**, *21*, 1125.
(54) Eberhard, J.; Howard, C. J. *Int. J. Chem. Kinet.* **1996**, *28*, 731.
(55) Tauzon, E. C.; Atkinson, R. *Int. J. Chem. Kinet.* **1990**, *22*, 1221.
(56) Chen, X. H.; Hulbert, D.; Shepson, P. B. *J. Geophys. Res., [Atmos.]* **1998**, *103*, 25563.
(57) Atkinson, R.; Aschmann, S. M. *Int. J. Chem. Kine.* **1984**, *16*, 1175.
(58) Ohta, T. *J. Phys. Chem.* **1983**, 87, 1209.
(59) Edney, E. O.; Kleindienst, T. E.; Corse, E. W. *Int. J. Chem. Kinet.* **1986**, *18*, 1355.
(60) Cox, R. A.; Derwent, R. G.; Williams, M. R. *Environ. Sci. Technol.* **1980**, *14*, 57.
(61) In the first report of this result, the wavelength of the atomic line for Cd(g) was misquoted because of a typographic error as 228.1 nm. The correct value is 228.883 nm.[37] The cross sections reported then and in this paper are at this wavelength. We regret the error.